Magnetic behavior of nanostructured films assembled from preformed Fe clusters embedded in Ag

C. Binns and M. J. Maher
Department of Physics and Astronomy, University of Leicester, Leicester LE1 7RH, United Kingdom

Q. A. Pankhurst
Department of Physics and Astronomy, University College London, London WC1E 6BT, United Kingdom

D. Kechrakos and K. N. Trohidou
Institute of Materials Science, NCSR "Demokritos," 15310 Athens, Greece

(Received 22 June 2002; revised manuscript received 12 September 2002; published 13 November 2002)

We have observed the magnetic behavior of nanostructured magnetic materials produced by co-depositing pre-formed Fe nanoclusters from a gas aggregation source and Ag vapor from a Knudsen cell. Films containing particle volume fractions from $<1\%$ (isolated clusters) to 100% (pure clusters with no matrix) have been prepared in UHV conditions and, after capping with a thin Ag layer for removal from the deposition chamber, have been studied at temperatures in the range 2–300 K by magnetometry and field-cooled/zero-field-cooled measurements. The results have been interpreted with the help of a Monte Carlo simulation of the cluster-assembled films that includes exchange and dipolar interactions. At elevated temperatures (>50 K) the lowest concentration films display ideal superparamagnetism with an H/T scaling of the magnetization. With increasing cluster density the films pass through an interacting superparamagnetic phase in which the effective blocking temperature and the initial susceptibility above the blocking temperature increase, in contrast to predictions of nanoparticle systems interacting via dipolar forces only. It is concluded that the exchange interaction becomes important even at volume fractions of 10% as clusters that are in contact behave as a single larger particle. This is confirmed by the theoretical model. At high volume fractions, well above the percolation threshold, the cluster assemblies form correlated superspin glasses (CSSG's). At 2 K, the magnetization curves in all films, irrespective of cluster concentration, have a remanence of $\approx 50\%$ and an approach to saturation that is characteristic of randomly oriented, particles with a uniaxial anisotropy, in agreement with the remanence. In the most dense Ag-capped films there appears to be a ''freezing out'' of the interparticle exchange interaction, which is attributed to temperature-dependent magnetoelastic stress induced by the capping layer. An uncapped 100% cluster film measured in UHV remains in the CSSG state at all temperatures and does not show the low-temperature decoupling of particles evident in the Ag-capped samples.

DOI: 10.1103/PhysRevB.66.184413 PACS number(s): 75.50.Tt, 75.50.Lk, 75.75.+a

I. INTRODUCTION

For decades, assemblies of interacting magnetic nanoparticles have been a fascination and a challenge for materials scientists. The isolated noninteracting nanoparticles are themselves interesting, behaving as giant moments of ferromagnetically coupled atomic spins whose vector fluctuates over the intraparticle anisotropy barrier in time scales ranging from nanoseconds to aeons.[1,2] Reversal can also occur via quantum-mechanical tunneling.[3–5] For particles smaller than about 5 nm, either as free clusters or supported on a surface the fundamental spin and orbital moments per atom can be substantially increased over the bulk value.[6–11]

When the interparticle interactions become significant the system displays a rich variety of magnetic configurations resulting from competing energy terms. The dipolar interaction introduces frustration as it is impossible to produce an optimum alignment for every particle. In addition there is frustration resulting from the competition between the interparticle dipolar and exchange terms and the intraparticle anisotropy energy (magnetocrystalline, shape, magnetoelastic, etc.) that requires the magnetization vector to be aligned along specific axes in each particle.

Developing a detailed understanding of the interactions is important not only to satisfy scientific curiosity but also in order to fully exploit such systems in the development of high performance magnetic materials.[12] In applications such as high-moment soft materials,[13] or magnetic sensors,[14] the required volume fraction of nanoparticles is close to or above the percolation threshold and is well into the strong interaction regime.

Experimentally the problem has been addressed for almost 30 years using a variety of measurement techniques, including magnetometry, susceptilibilty measurements, muon spin resonance, and Mössbauer spectroscopy and samples including frozen ferrofluids, co-sputtered metal/insulator films, annealled melt spun alloys, and ball-milled alloys.[15–30] A detailed picture has developed of fine particle magnetism and a deep understanding of both the superparamagnetic state, discussed by Néel,[2] and the blocked state. When considering the modifications to these states resulting from the interactions between the particles, although each work develops a successful model to account for the magnetic behavior, several fundamental inconsistencies are apparent when comparing different experiments. For example, in the limit of small interaction, there is some debate as to whether the dipole-dipole interaction between particles decreases or increases the relaxation rate.[17,23] In addition while some ex-

periments detect an increase in the apparent blocking temperature with the onset of interaction,[17–22] other results show the opposite trend.[23] For blocked particles the remanence also is found to either increase[18,21] or decrease[24] relative to the isolated cluster case when interactions become significant. A recent Monte Carlo simulation[31] considering the dipolar interaction between the particles has shown that within a certain range of the dipolar/anisotropy energy ratio, the remanence of the low-temperature assembly can increase and then decrease with increasing volume fraction of particles.

Considering the complexity of the system such contradictions are not surprising. The experimental data has been obtained from systems produced by a variety of different techniques and undoubtedly some of the conflicting results arise from subtle differences in the particle assemblies including the particle morphology and size distribution. We believe a crucial difference is that some production methods guarantee a nonmagnetic shell around each magnetic core (cluster, particle, or granule) while others allow the cores to come into direct contact. Some methods, for example annealing melt spun films, may produce either situation depending on the experimental conditions. This can make a profound difference to the magnetic properties since a nonmagnetic shell will exclude the direct exchange interaction between particles so that the dipole force dominates at all achievable volume fractions. If, on the other hand, the clusters are allowed to touch and are arranged randomly, neighbors will start to come into contact invoking a strong exchange interaction at low volume fractions. For example in an assembly with a 10% volume fraction, irrespective of the particle size, the majority of the clusters will be in contact with at least one neighbor.

A recent study of nanocrystalline films of pure Fe produced by ball milling[32] revealed a more subtle exchange decoupling mechanism without the need for a nonmagnetic shell. It was proposed that the interface between grains is amorphous and that at a sufficiently low temperature this interface forms a spin glass that does not transmit exchange. Thus even for particles in contact the detailed nature of the interface is important. We demonstrate a similar low-temperature decoupling in dense cluster films that we attribute to a large increase in the intraparticle anisotropy at low temperature due to stress rather than a removal of exchange.

Here we report a wide-ranging study of cluster assemblies produced by co-depositing preformed Fe nanoclusters (from a gas aggregation source) with the Ag vapor in UHV conditions. In this production system the volume fraction can be controlled independently of the cluster size and the clusters can come into direct contact. The size distribution of the clusters and their individual behavior has been determined by previous experiments so we have a good understanding of the basic building blocks of the films. We have produced samples with volume fractions that vary from the dilute limit, in which the interaction is negligible and the isolated cluster properties are apparent, to cluster films with no matrix in which every cluster is in contact with its neighbors. This has allowed us to build up a detailed picture of the behavior of the interacting nanoparticles. Several landmark papers on the magnetic behavior of deposited nanoclusters have been published.[33–38] In this paper we chart the evolution of the magnetic behavior as the volume fraction is varied between the two extremes. We compare the results with a Monte Carlo simulation that includes both dipolar forces and the exchange interaction between particles that are in contact.

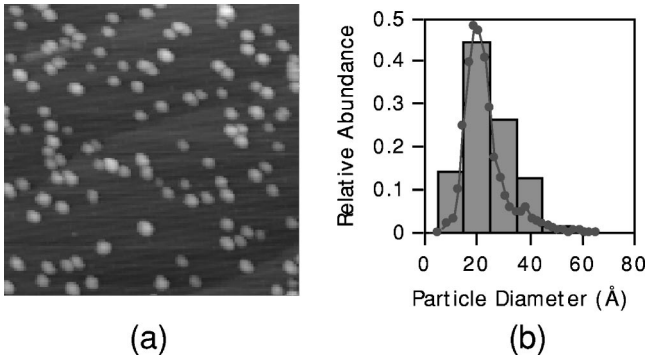

FIG. 1. (a) STM image (100×100 nm) of unfiltered Fe clusters on Si(111). (b) Height distribution from STM images (dots+line) compared with a size histogram from Langevin fits to the magnetization of dilute cluster films at $T\geqslant50$ K.

II. FILM PREPARATION AND MEASUREMENTS

Fe nanoclusters were formed using a UHV-compatible gas aggregation source.[39] These were co-deposited onto polyether-ether-ketone (PEEK) films with Ag supplied by a conventional Knudsen cell evaporation source. Sample areas were approximately 10×10 mm. For *ex situ* experiments the films were capped with a 5-nm protection layer of Ag.

Magnetization isotherms were obtained using a vibrating sample magnetometer (VSM) operating at fields of up to 9 T and temperatures down to 1.5 K and the field-cooled (FC)/zero-field-cooled (ZFC) measurements were carried out using a superconducting quantum interference device (SQUID) magnetometer. One film of pure clusters (S10) was also prepared without the capping layer by depositing directly onto a PEEK rod that could be sealed *in situ* in a PEEK ampoule and transferred into the VSM without breaking vacuum. The system has been thoroughly tested and proven to maintain uncapped films without any detectable contamination. Figure 1(a) shows an *in situ* scanning tunnel microscope (STM) image of unfiltered Fe clusters deposited onto a Si(111) $-(7\times7)$ surface at 300 K.[40] The main points emerging from the image are the pseudospherical morphology of the particles (some faceting is evident), the narrow size distribution, and the nature of the contact between particles. When particles touch they do not coalesce but stay as distinct grains and tend to contact along the facets. It is clear that there will be a strong exchange interaction between touching neighbors. The cluster height distribution obtained using the STM is drawn as a line in Fig. 1(b) and shows a log-normal shape with a most probable height of 2 nm and a standard deviation of 1. Superimposed on this curve is a histogram of the ''magnetic size'' distribution obtained by fitting Langevin functions to the ($T\geqslant50$ K) magnetization curves of Fe clusters,

TABLE I. Samples reported in this study. All films contain Fe clusters with a log-normal size distribution peaking at 2.5 nm and a standard deviation of 1.5 (see Fig. 3). A quoted volume fraction of 100% refers to films of pure clusters with no matrix.

Sample	Fe Volume fraction (%)	Totalfilm thickness (nm)	Capping layer
S1	0.8 ± 0.2	850 ± 150	5-nm Ag
S2	10 ± 2	39 ± 8	5-nm Ag
S3	16 ± 3	78 ± 16	5-nm Ag
S4	19 ± 4	135 ± 25	5-nm Ag
S5	25 ± 5	36 ± 7	5-nm Ag
S6	42 ± 8	20 ± 4	5-nm Ag
S7	70 ± 14	7 ± 1.5	5-nm Ag
S8	100	15 ± 3	5-nm Ag
S9	100	3 ± 0.6	5-nm Ag
S10	100	5 ± 1	no capping layer

produced by the source operating under the same conditions, embedded in Ag with a 1% volume fraction. The agreement between the two distributions shows that the cluster size distribution is unchanged by embedding in matrices and the clusters in the matrix can be assumed to have a similar morphology to those imaged directly in Fig. 1(a).

The STM images are unable to determine whether there is any flattening of the clusters, which may occur even at the low deposition energies used here.[41] The low-temperature magnetization curves of Fe clusters embedded in Ag are, however, nearly the same in the out-of-plane direction as in-plane[42] indicating minimal shape anisotropy. The agreement between the observed size with the STM and the magnetic size of the embedded clusters demonstrates that there is no large scale interdiffusion of the Fe and Ag though some intermixing at the interface cannot be ruled out. An extended X-ray-absorption fine structure (EXAFS) study of 3-nm Co nanoparticles embedded in Ag produced by the cluster deposition technique has shown that the interface is sharp with no intermixing.[43] All films were prepared under UHV conditions and numerous *in situ* x-ray magnetic circular dichroism (XMCD) studies of films prepared in the same way have revealed no trace of oxide. We cannot, however, rule out limited oxidation after removal from the system due to imperfections in the capping layer.

The size distribution shows the same characteristic shape irrespective of the conditions within the source but running with different bath gas pressures allows some control over the most probable size and the width of the mass spectrum. As shown in Sec. IV B, for all the samples reported here the most probable diameter is 2.5 nm with a standard deviation of 1.5 giving a median diameter of 3 nm. The film thickness, volume fraction, and capping layer for each sample is listed in Table I. In practice the aim was to include at least a 5-nm equivalent thickness of Fe clusters irrespective of volume fraction to obtain a good signal in the VSM. Often the depositions were continued longer and the Fe equivalent thicknesses extend to 25 nm apart from sample S9, which was deliberately prepared as a cluster monolayer.

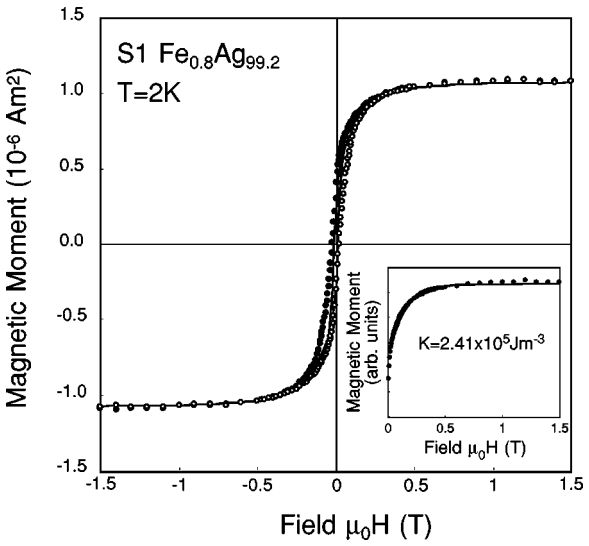

FIG. 2. Magnetization isotherm at 2 K of $Fe_{0.8}Ag_{99.2}$. Open (closed) symbols are the data for the field sweeping up (down). The thin solid line is a simulation using the MC model. The inset shows the data sweeping down from saturation to remanence (dots) compared to a fit using Eq. (2) that assumes the particles have a uniaxial anisotropy and a random alignment of anisotropy axes (line). The anisotropy constant for the optimum fit is shown.

III. THEORETICAL MODEL AND SIMULATION METHOD

To model the films we consider N identical magnetic particles (grains), with spherical shape and diameter D inside a cubic box of edge length L. For simplicity, the space inside the box is discretized by a simple cubic lattice with a lattice constant equal to the particle diameter. Particles are placed at random on the nodes of the lattice, thus overlap is avoided.[44] The single-domain particles have a random uniaxial anisotropy and they interact via long-range dipolar forces and short-range exchange forces. The latter are included only between neighboring particles in contact. The total energy of the system is the sum of particle magnetic energies, $E=-\Sigma_i \epsilon_i$, in which the energy of the ith particle is

$$\epsilon_i = h(\hat{s}_i\cdot\hat{H}) + k(\hat{s}_i\cdot\hat{e}_i)^2 + g\sum_j \frac{3(\hat{s}_i\cdot\hat{R}_{ij})(\hat{s}_i\cdot\hat{R}_{ij})-(\hat{s}_i\cdot\hat{s}_j)}{R_{ij}^3} + J\sum_{\langle j\rangle}\hat{s}_i\cdot\hat{s}_j, \tag{1}$$

where $\hat{s}_i$ and $\hat{e}_i$ are unit vectors in the directions of the magnetic moment (spin) and anisotropy axis of the ith particle and $\hat{R}_{ij}\cdot D$ is the center-to-center distance between the particles. The energy parameters entering Eq. (1) are the Zeeman energy, $h=\mu H$, the dipolar energy, $g=\mu_0\mu^2/4\pi D^3$, the anisotropy energy, $k=KV$, and the effective exchange energy J. The Fe particles in all samples have a median diameter of $D=3.0$ nm, a magnetic moment $\mu=2.44\times10^{-20}$ A m^2 and an anisotropy energy density $K_1=2.4\times10^5$ J m^{-3} (Figs. 2 and 3). The value of J can be directly extracted from the correlated spin glass fits to the high volume fraction samples (see Sec. IV E) and is found to be

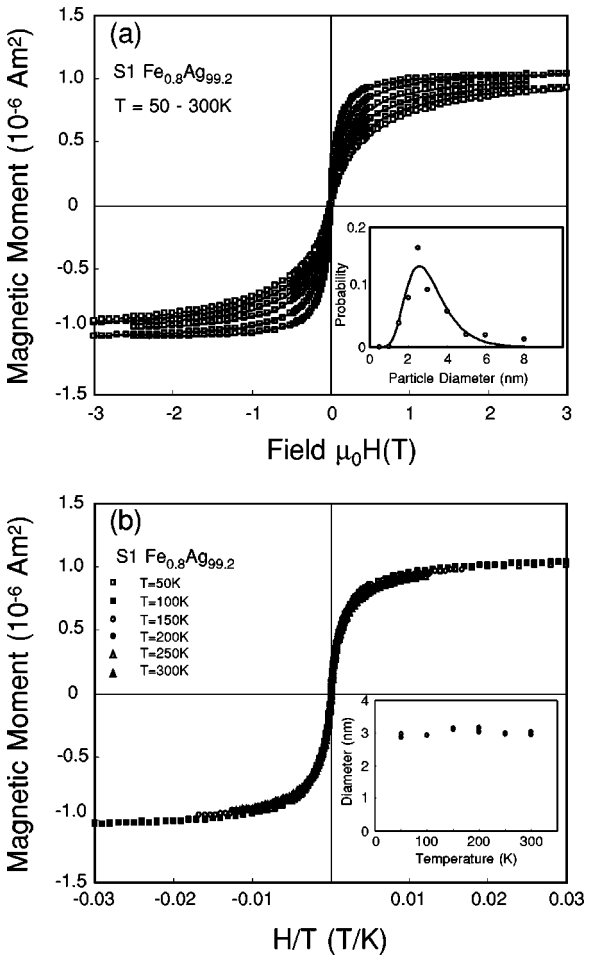

FIG. 3. (a) Magnetization isotherms in the range 50–300 K of $Fe_{0.8}Ag_{99.2}$ (open squares) compared to fits by Langevin functions (lines) with a size distribution represented by ten size bins in the range 0.5–8 nm. The inset shows the average probability of each bin for the optimum fit to curves at temperatures >50 K (open circles) and the corresponding log-normal distribution (line) with $d_{max}=2.57$ nm and $\sigma=1.95$. (b) The same data plotted against H/T showing the scaling predicted by the Langevin functions. The inset shows the median size from the distributions as a function of temperature and demonstrates the invariance of the fitted size vs T required for an ideal superparamagnetic system.

3.11×10^{-20} J. The equilibrium magnetic configuration of the system at a certain temperature and applied field is obtained by a Monte Carlo (MC) simulation using the Metropolis algorithm.[31] The model predicts a percolation threshold at a volume fraction (VF) of 29% and that the dilute limit extends up to about 5%, where the probability of particles in contact is small. The intermediate volume fraction regime covers the range VF=5–25%. In all simulations it is assumed that the morphology of the Fe clusters does not change with volume fraction.

IV. RESULTS

A. Dilute cluster film below the blocking temperature

Initially we will consider the behavior of the most dilute sample, S1 ($Fe_{0.8}Ag_{99.2}$), to develop a detailed understanding of the magnetic behavior of the noninteracting clusters. The isotherm at 2 K of Sample S1 is shown in Fig. 2. The blocking temperature for the median cluster size is 5 K (see below) and so at 2 K the sample displays hysteresis. In an assembly of noninteracting particles with uniaxial anistropy, randomly oriented in three dimensions, the magnetization between saturation and remanence is obtained at each field value by minimizing over all alignments of the anisotropy axes the intraparticle energies:

$$E_\phi = KV\sin^2(\phi-\theta)-\mu_B\cos\phi, \tag{2}$$

where K is the anisotropy constant, V is the particle volume and θ and ϕ are the angles between the applied field and the anisotropy axis and particle magnetization vector, respectively. It is evident from the inset in Fig. 2 that this simple model reproduces the data accurately. So in zero field the system is a collection of static, randomly aligned cluster giant moments each pointing along the local anisotropy axis. The anisotropy constant is a parameter of the fit and optimizes at $K=2.41\times10^5$ J m^{-3}, which is close to the value of $K=2.3\times10^5$ J m^{-3} obtained by a previous SQUID measurement of a similar sample,[45] and is about five times the bulk value. The measured cluster anisotropy is used in the MC simulation. The particle diameter is shown below to have a most probable value of 2.5 nm and a median value of 3 nm thus the blocking temperature can be evaluated to be ≈5 K.

The measured remanence is $\approx40\%$, which is slightly less than the value of 50% predicted for a noninteracting uniaxial assembly. Higher symmetry than uniaxial, e.g., cubic, produces a remanence higher than 50% as does averaging moments over two rather than three dimensions. Neither can the low remanence be ascribed to interactions as we show below, unambiguously, that they are insignificant in this sample. The reduced remanence compared to the ideal case is ascribed in part to the smallest particles in the film remaining unblocked at 2 K. With the anisotropy derived above, this will be the case for particles smaller than 1.8 nm. Inspection of the size distribution reveals that about 10% in the population will remain unblocked at 2 K, predicting a remanence of 45%. The remaining discrepancy probably arises from a variation of the anistropy with cluster size.

Inserting the anisotropy value obtained from the simple fit using Eq. (2) into the MC model described in Sec. III allows one to calculate the complete magnetization curve, which is shown as a thin solid line in Fig. 2. This describes the data reasonably well and gives a good estimate of the coercive field (0.02 T). The main discrepancy is the loss of hysteresis at a lower field than observed in the data. We believe this is due to the fact that the model describes each particle by a single average spin whereas for isolated particles the surface spins need a higher field than the core to saturate because of the enhanced surface anisotropy. At higher concentrations where the interparticle interactions are dominant the surface contribution is less important and the model gives even better agreement.

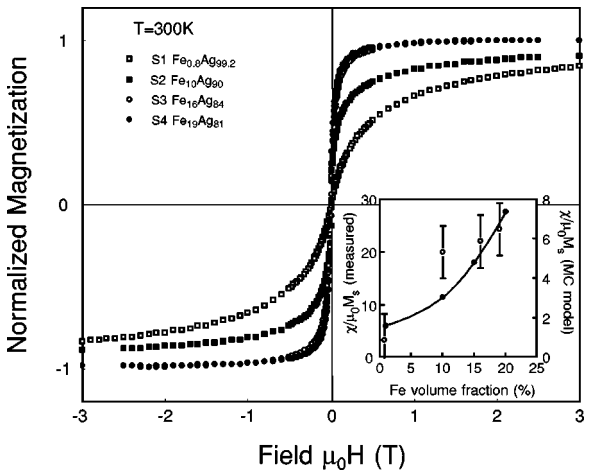

FIG. 4. Magnetization isotherms at 300 K of films as a function of volume fraction in the intermediate range. The inset compares the measured initial susceptibility with that calculated by the MC simulation as a function of volume fraction (note the different scales).

B. Dilute cluster films above the blocking temperature

Figure 3(a) shows a set of isotherms from sample S1 (symbols) taken at temperatures in the range 50–300 K. The inset shows a stacked area plot of the size distribution obtained by fitting Langevin functions in 10 size bins in the range 0.5-8nm to each isotherm. The calculated curves are displayed as lines and the fit is excellent in every case. The size distribution is the usual asymmetric shape and fitting it to a log-normal distribution gives a most probable cluster size of 2.5 nm with a standard deviation of 1.5. It was pointed out by Allia,[29] however, that this procedure is hazardous. In an interacting system it is possible to obtain an excellent Langevin fit with an ''apparent size'' that is different from the real size and varies with temperature. We can therefore devise three tests to demonstrate ideal superparamagnetism with no interactions in this sample: (a) the isotherms should display no hysteresis, (b) they should scale with H/T, and (c) the fitted size distribution should be independent of temperature. The lack of hysteresis is evident and the other two conditions are demonstrated in Fig. 3(b), which is the data in Fig. 3(a) re-plotted against H/T and an inset that shows the invariance with temperature of the median size obtained from the Langevin fits. This sample thus displays perfect superparamagnetism.

C. Interacting cluster films below the percolation threshold—elevated temperature behavior

The evolution of the magnetization curves at 300 K as a function of volume fraction is shown in Fig. 4. The most noticable feature is the increase of the low-field susceptibility as the cluster density increases. This is characteristic of larger particles and indeed it is possible to get good fits using Langevin functions with a higher supermoment than in the dilute film. It is, however, erroneous to treat these films as superparamagnetic with a volume fraction-dependent cluster size. The magnetic isotherms do not scale with H/T and

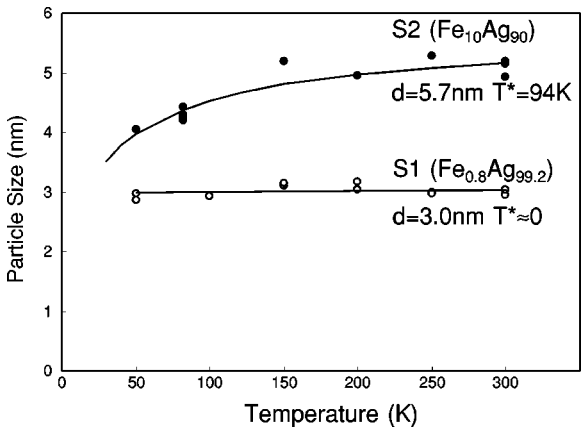

FIG. 5. Median particle diameter d obtained by fitting unmodified Langevin functions to the magnetization curves taken at 50–300 K of sample S1 ($Fe_{0.8}Ag_{99.2}$—open symbols) and S2 ($Fe_{10}Ag_{90}$—solid symbols). The variation of d vs T can be used to obtain the interaction parameter T^* from Eq. (4).

Langevin fits to these curves give an optimum particle size that depends on the temperature of the fit ($\sim$20% variation from 50–300 K—see Fig. 5) and so the criteria for superparamagnetic behavior are not satisfied.[29] The best description (see below) is that the particles are in exchange coupled aggregates, which, below the percolation threshold, interact via dipolar forces. Following Allia *et al.*,[29] the dipolar interactions can be characterized by a parameter T^*, proportional to the rms dipolar energy, appearing in the denominator of a modified Langevin function analogous to the Curie-Weiss law, that is,

$$M = N\mu L\left(\frac{\mu H}{k(T+T^*)}\right), \tag{3}$$

where μ is the true particle (aggregate) moment. From this one can obtain that the true diameter d is related to the apparent diameter d_a obtained by fitting simple (superparamagnetic) Langevin functions to the magnetization curves, by

$$d_a = \left(\frac{1}{1+\frac{T^*}{T}}\right)^{1/3} d. \tag{4}$$

The variation of d vs temperature is shown in Fig. 5 for samples S1 ($Fe_{0.8}Ag_{99.2}$) and S2 ($Fe_{10}Ag_{90}$). For the dilute clusters no significant varation with cluster size can be observed and fits using Eq. (4) give T^* less than the single-particle blocking temperature. For S2 the variation is well described by Eq. (4) and one obtains $T^* = 94$ K and a mean aggregate diameter of 5.7 nm. Thus on average the aggregates consist of 6–7 of the deposited nanoclusters exchange coupled and behaving as individual larger particles. These interact via dipolar forces, the strength of which is characterized by T^*. The value of T^* is reasonable for particles of this size.[29]

We can use the MC simulation including the exchange interaction between neighboring grains to test that the mag-

netization curves evolve as in Fig. 4 with increasing volume fraction but first it is important to point out some expected differences between the measured data and the simulation. In a MC simulation, due to the absence of true spin dynamics, the physical time does not enter directly, but instead ''time'' is measured in Monte Carlo steps (MCS). Our simulations extend to 10^4 MCS per spin, which approximately correspond to an observation time of $t_{MC} \sim 10^{-7} s$.[44] Consequently, the MC simulation for the dilute sample ($p=1\%$) predicts a much higher blocking temperature ($T_b^{MC}=32$ K) than the experimental value ($T_b^{exp}=5$ K). Comparing the measured and simulated data is thus similar to comparing measurements with widely different time scales, for example dc magnetometry and Mössbauer spectroscopy. However, the MC simulation, because it mimics the role of thermal fluctuations, reproduces qualitatively the trend of the experimental data. The trend in the initial susceptibility as the volume fraction changes for the experimental data is plotted in the inset in Fig. 4 and compared with the prediction from the MC model. It is seen that there is qualitative agreement with the model. Theoretical modeling[46] and measurements[29] show that without exchange, dipolar forces decrease the low-field susceptibility emphasizing the importance of including exchange interactions to explain the behavior of our samples.

Figure 6 shows how the FC/ZFC curves in the temperature range 10–300 K develop with increasing volume fraction up to 25%. In a superparamagnetic system a peak in the ZFC curve marks the blocking temperature at the time scale of the measurement (100 s in this case). For the very dilute sample the temperature does not go down to the blocking temperature of 5 K so the peak is not observed but the curves follow a $1/T$ dependence as required. With increasing volume fraction a peak does occur and, as with the magnetization data, without other measurements, it would be tempting to interpret the curves in terms of a superparamagnetic system with an increased average particle size resulting from clusters in contact. As shown above, however, all samples with an Fe volume fraction of 10% and greater are not superparamagnetic.

This is also evident in the shape of the FC/ZFC curves that show a severe flattening at high temperature with respect to the ideal superparamagnetic system (S1). In addition the temperature at which the peak in the ZFC curves occurs varies more rapidly with the applied field than would be observed in a superparamagnetic system. This variation was calculated by Dormann *et al.*[47] who showed that for isolated particles in an applied field H the reduced blocking temperature, given by $t_r = 1 - T_b(h)/T_B(0)$, is proportional to $h^{2/3}$ where h is the reduced field, $h = \mu H/2E_0$. Here μ is the particle moment and E_0 is the anisotropy energy barrier given by KV. We can use the known particle volume and the observed anisotropy constant (Fig. 2) to obtain, for the isolated particles, $E_0 = 3.4 \times 10^{-21}$ J. So in the range $H = 100$–500 G, $h^{2/3} = 0.11$–0.32 and for isolated particles, a 20% variation in T_b should be observed. In fact a slightly smaller variation would be expected since the lowest h value is in the ''low-field'' regime where the variation of T_b with H is slower. The MC model for the isolated clusters gives a

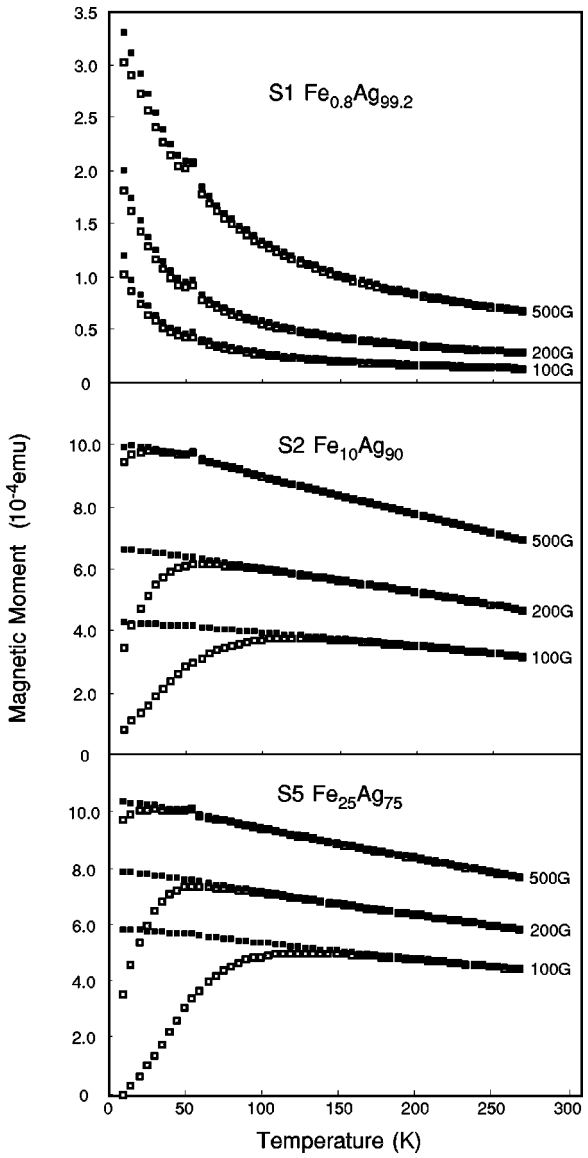

FIG. 6. Measured FC/ZFC curves as a function of volume fraction in the intermediate range.

17% decrease in the peak position of the ZFC curve as the measuring field is increased from 100 to 500 G and is consistent with the superparamagnetic model of Dormann *et al.* Describing the behavior of the FC/ZFC data in the interacting systems requires the MC simulation with exchange and dipolar coupling. Due to the difference in timing outlined above the peaks in the modeled curves will not agree quantitatively with the experimental data but we can look for trends. As shown in Fig. 7, the $1/T$ dependence of the magnetization is lost due to the presence of strong exchange ($J = 3.11 \times 10^{-21}$ J) between the particles. The inclusion of magnetostatic interactions is necessary to produce the almost linear decay of the magnetization observed for volume fractions above 10%. The peak in the ZFC curve, which is interpreted as the blocking temperature, is shifted to higher values due to the presence of both types of interaction. We have performed simulations without the magnetostatic interaction (not shown here) and we have found a much weaker

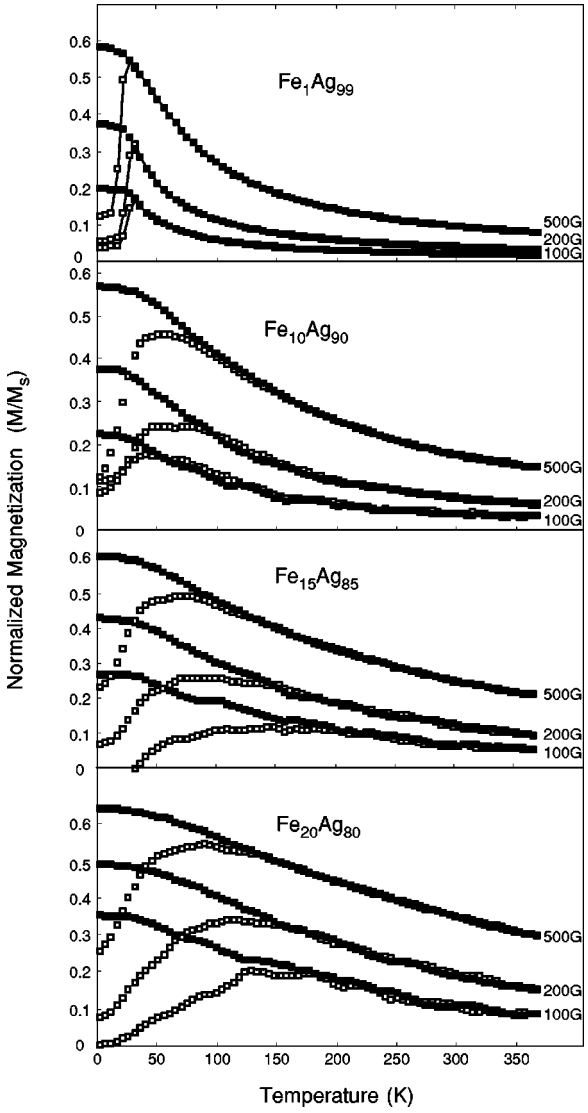

FIG. 7. Simulated FC/ZFC curves for Fe nanoparticle systems with intermediate volume fractions. Lines have been included in the Fe_1Ag_{99} ZFC curves to guild the eye.

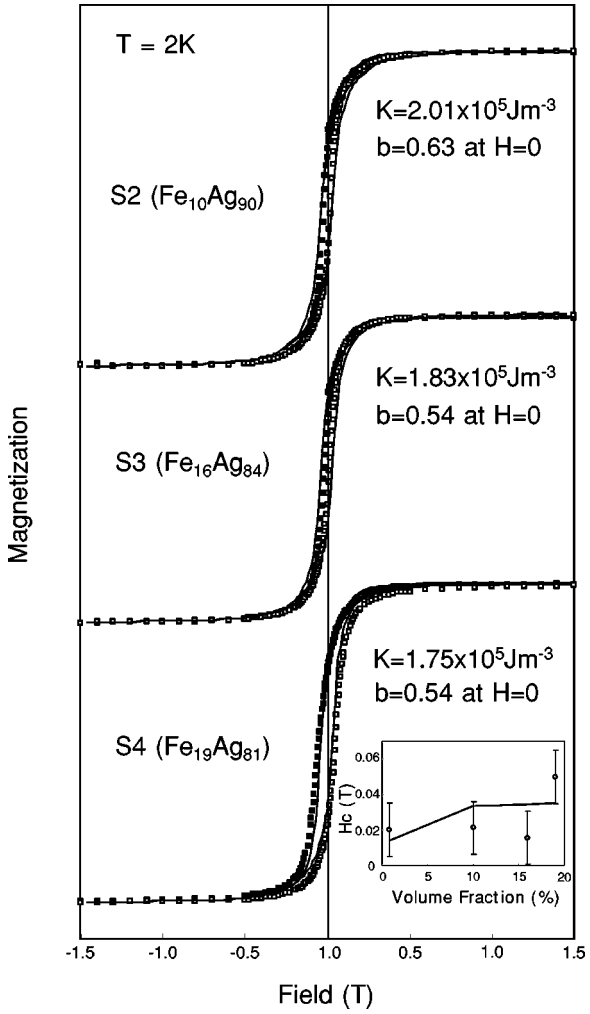

FIG. 8. Isotherms at 2 K from samples with intermediate volume fractions below the percolation threshold. The symbols are the measured data and the thick lines are fits between saturation and remanence using Eq. (2) with the optimal value of the anistropy constant shown. The thin solid lines are the MC simulations for the full isotherms with the predicted value of b at remanence shown. The inset compares the values of H_c obtained from the measurements and the MC simulation.

field dependence of the blocking temperature. Therefore magnetostatic interactions are necessary to explain the large shifts of the apparent blocking temperature with applied field in our samples. The FC/ZFC data and simulations are in agreement with the picture presented above, that is, the exchange interaction couples individual clusters into aggregates giving the increase in T_b and the aggregates interact via dipolar forces that produce the strong field dependence of the peak in the curves and the flattening at high temperatures.

D. Ground state of interacting cluster films below the percolation threshold

Figure 8 shows the magnetization isotherms at 2 K as a function of the Fe cluster volume fraction for values below the percolation threshold. In each case the demagnetization from saturation is still well described using Eq. (2) (thick solid lines in Fig. 8) and the remanence is close to 50% indicating that at 2 K in zero field the moments in the aggregates are frozen along the randomly oriented anisotropy axis of each aggregate, which is uniaxial as in the isolated clusters. The optimal anisotropy obtained by fitting to Eq. (2) is lower in the $Fe_{10}Ag_{90}$ film than that found in the isolated clusters and decreases with increasing density of clusters. This is expected due to an averaging of the individual cluster anisotropies to produce a resultant value along the anisotropy axis of the whole aggregate. In addition a real decrease in the intracluster magnetocrystalline anisotopy may be expected as a result of a decreasing orbital moment with density as shown by previous XMCD measurements on exposed Fe clusters on graphite.[8]

Later we present evidence that in the very high volume fraction samples, at 2 K the moments of the individual clusters decouple and the magnetization in each points along the local cluster anistropy axis. Although we cannot rule this out

here from the magnetization data alone, the MC simulation indicates that the clusters in the aggregates are exchange coupled. From the simulation, one obtains the parameter

$$b = \frac{1}{N} \sum_i |\hat{s}_i \cdot \hat{e}_i|, \tag{5}$$

that is, the fraction of projected moments along the local easy axes. A value of 1 indicates complete decoupling of clusters so that all moments are along local easy axes and 0.5 will be found in the case where all neighboring moments are aligned colinearly by exchange. For the dilute cluster film, it is found that $b=0.89$ at $H=0$ and $T=5$ K but drops to 0.63 in sample S2 ($Fe_{10}Ag_{90}$) and drops further towards the exchange coupled limit as the Fe cluster volume fraction increses. The thin solid lines in Fig. 8 are the MC simulation of the magnetization curves and there is good agreement.

The simulation also gives a good estimate of the coercive field and predicts the experimental observation of a slight increase with increasing Fe volume fraction. The large error bars for the experimentally determined values of H_c are due to uncertainties in the removal of the background slope from the raw data. The variation of H_c with volume fraction is due to the different character of the dipolar interactions in the system well below and close to the blocking temperature. For $T \ll T_b$, H_c is predicted to decrease with increasing volume fraction while for $T \sim T_b$ it will increase. This is clearly the regime found in our samples. More fundamentally, it is evident that H_c is modified by interactions as it is observed to increase despite a decreasing anisotropy constant in the aggregates. This would be a contradiction in a noninteracting system.

E. High volume fractions—the formation of correlated spin glasses

As the volume fraction is increased further, beyond the percolation threshold, at 2 K, the magnetization curves continue to show a remanence of 50% and the magnetization between saturation and remanence is accurately described by Eq. (2), which assumes a random orientation of moments with a uniaxial anisotropy. This is the case even for the pure cluster film containing no matrix, as shown in Fig. 9. The data is modeled by the same curve (apart from a change in the optimal anisotropy constant) as the dilute cluster film (sample S1, Fig. 2). What is not clear from the data is the length scale of the random moments, i.e., is it on the scale of individual particles or is the moment correlated over aggregates of several particles. The picture used in the lower volume fraction samples, for example $Fe_{10}Ag_{90}$ (sample S2), of aggregates separated by the nonmagnetic matrix is not valid in pure cluster films. We will return to this question later after considering the data at higher temperatures.

The similarity between the films with different volume fractions of Fe clusters vanishes at elevated temperatures. As shown in Fig. 9(b) the magnetization curve at 300 K shows a high susceptibility at low fields in contrast to the data for the isolated clusters. Hysteresis also disappears as in the superparamagnetic case but it is not possible to get a good fit using Langevin functions with any reasonable size distribution. Instead, as shown in the inset in Fig. 9(b), the approach to saturation is accurately described by a correlated superspin glass (CSSG) state predicted by a random anisotropy (RA) model developed by several authors in the last two decades.[48–51]

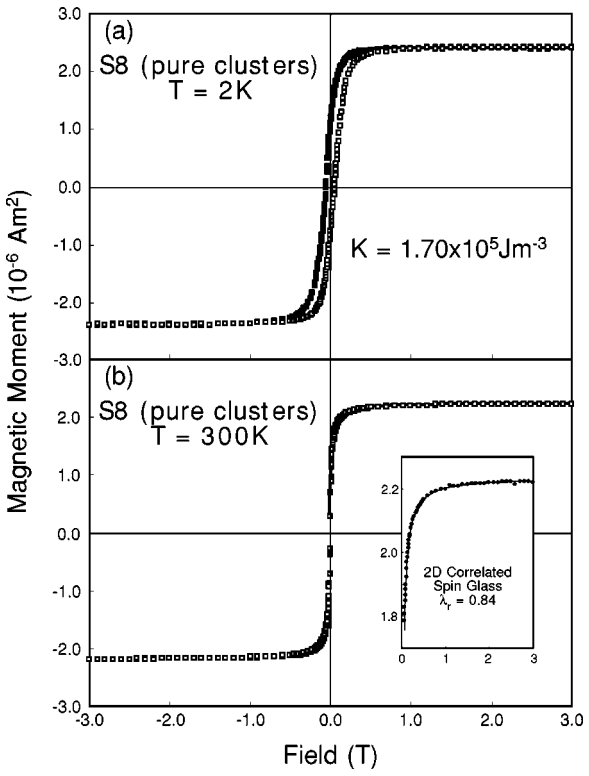

FIG. 9. (a) Magnetization isotherm at 2 K of sample S8 (pure clusters) The symbols are the measured data and the line is a fit using Eq. (2) with the anisotropy constant shown. (b) Magnetization isotherm at 300 K of sample S8 (pure clusters). The symbols are the measured data and the line is a fit to the approach to saturation predicted for a two-dimensional correlated spin glass with the λ_r parameter shown (see text). The inset details the approach to saturation.

In the RA formalism, the magnetic ground state in a granular film is determined by the relative strength of a random anisotropy field:

$$H_r = \frac{2K_r}{M_s}, \tag{6}$$

and an exchange field:

$$H_{ex} = \frac{2A}{M_s R_a^2}, \tag{7}$$

where K_r is the (randomly oriented) anisotropy of the grains, M_s is their saturation magnetization, A is the exchange constant for the interaction between the grains, and R_a is the nanometer-sized region over which the local anisotropy axis is correlated, i.e., the characteristic grain size. Their relative strength is given by the dimensionless parameter

$$\lambda_r = \frac{H_r}{H_{ex}} = \frac{K_r R_a^2}{A}. \quad (8)$$

The model was developed to describe amorphous films in which a local, randomly oriented, anisotropy is due to local atomic order. It is even better suited to providing a description of the magnetization in cluster-assembled films in which the distance R_a over which an anisotropy axis is correlated is well defined (i.e., the particle diameter). In addition, as pointed out by Löffler *et al.*,[35] the exchange interaction at the boundaries between particles is weaker than the intraparticle atomic exchange further reinforcing the image of seperate but interacting particles. The RA model has been used previously to analyze magnetization data from cluster-assembled films[33–35] but Löffler *et al.*[35] found that for assemblies containing larger particles (10–60 nm) the model has to be modified to allow for the formation of domain walls within the grains. That is not a relevant factor in the films reported here with a particle size of 3 nm.

For $\lambda_r > 1$ the magnetic correlation length at zero field is R_a, and the magnetic vector in each particle points along the local intraparticle anisotropy axis. Note that in an arrow representation this state would be identical to that in isolated noninteracting particles at absolute zero. With increasing interparticle exchange (or decreasing intraparticle anisotropy) the configuration becomes a correlated superspin glass (CSSG) in which the magnetization vector in neighboring particles is nearly aligned but the random deviation of the moments from alignment produces a smooth rotation of the magnetization throughout the system with a magnetic correlation length that is much larger than the particle diameter. The absolute value of λ_r marking the crossover between the two regimes depends on a number of factors including the angular distribution of the anisotropy axes, which may not be truly random. For example Löffler *et al.*[35] showed that a cluster-assembled film in which $\lambda_r = 2$ was in the CSSG state. The disordered CSSG state is fragile and application of a small field produces a ''ferromagnet with wandering axes'' (FWA) (Ref. 49) with an approach to saturation that follows a $1/\sqrt{H}$ dependence in three dimensions[49] and a $1/H$ dependence in two dimensions.[48] These both change to a $1/H^2$ dependence above a crossover field[51] $H_{co} = 2A/M_s R_a^2$.

Over the whole field range the approach to saturation was found to be best fitted by the two-dimensional (see later for a discussion of the dimensionality) FWA state given by[52]

$$M = M_s \left(1 - \frac{1}{32} \frac{\lambda_r^2}{\sqrt{h_{ex}}} \int_0^\infty dx C(x) x^2 K_1[x\sqrt{h_{ex}}] \right), \quad (9)$$

where $h_{ex} = H/H_{ex}$, K_1 is the modified Hankel function, and $C(x)$ is the correlation function for the anisotropy axes with x in units of R_a. In an amorphous metal, $C(x)$ will be a smoothly decreasing function with a characteristic decay distance of R_a. For example, $C(x) = \exp(-x^2/2)$ has been used in fits to three-dimensional (3D) spin glasses.[53] In a cluster-assembled film consisting of monosized particles, $C(x)$ will be a step function cutting off at $x = 1$.[54] Here we have rounded the step function by using $C(x) = \exp(-x^8/2)$ to simulate the narrow size distribution. Visually there is no discernible change to the fits if a simple step is used.

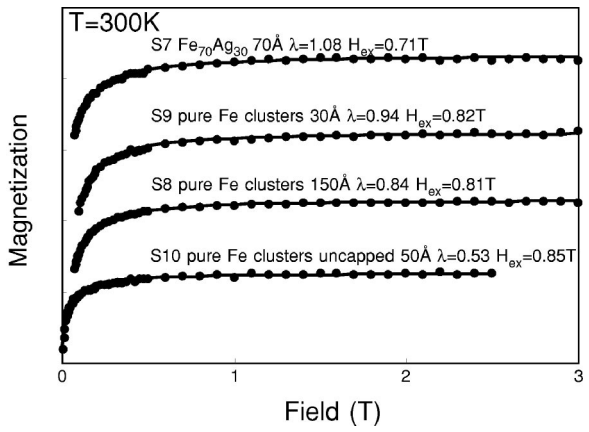

FIG. 10. Approach to saturation at 300 K of films S7–S10 compared to calculations using Eq. (9) for the FWA state (magnetized CSSG). The parameters λ_r and H_{ex} producing the best fit are displayed above each curve. Increasing the cluster density from 70% (S7) to 100% (S8 and S9) produces an increase in the exchange interaction between the clusters. The uncapped pure cluster film maintains a similar exchange interaction but shows a significant reduction in λ_r due to a decrease in the intraparticle anisotropy.

We have used the 2D expression for the approach to saturation since the cluster films analyzed with the RA model (S7, S8, S9, S10) are between 1 and 5 cluster layers thick. The 3D equivalent to Eq. (9) (Ref. 52) can also produce good fits to the data for S8, the thickest (~ 5 layers) film so this analysis alone is unable to detect the dimensional crossover of the CSSG but as shown below using Eq. (9) for all the films produces a consistent set of the fitting parameters, H_r and H_{ex}. Dimensional crossover has been demonstrated in thicker cluster-assembled films.[42]

Figure 10 shows the excellent agreement between the measured and calculated approach to saturation from $0.8M_s$ [using Eq. (9)] at 300 K for four different films of dense clusters along with the values of λ_r and H_{ex} producing the best fit in each case. There is a reduction of λ_r in going from the $Fe_{70}Ag_{30}$ film due to an increase in the exchange interaction in the denser film. The exchange field of ~ 0.8 T found for samples S8 and S9 corresponds to an exchange constant $A = 3.3 \times 10^{-12}$ J m^{-1}. This is lower than the value of $\sim 10^{-11}$ J m^{-1} used for bulk Fe but, as stated above, a lower average exchange interaction in the cluster-assembled film is expected.[35] For 3-nm particles (median diameter) this value of A gives an exchange energy, $J = 3.11 \times 10^{-20}$ J—this is the value used in the MC simulation. The exchange parameters for the Ag-capped 30-Å-thick (S9) and 150-Å-thick (S8) pure cluster films are similar. The uncapped pure cluster film (S10), while maintaining a similar exchange interaction between the clusters, shows a significant reduction of λ_r. This must be due to a drop in the random anisotropy parameter H_r and demonstrates that a significant contribution to the intracluster anisotropy in the other films is from the Ag capping layer, presumably from magnetoelastic stress. As the temperature is decreased to 50 K the fits to the data from the Ag-capped films (S7–S9)

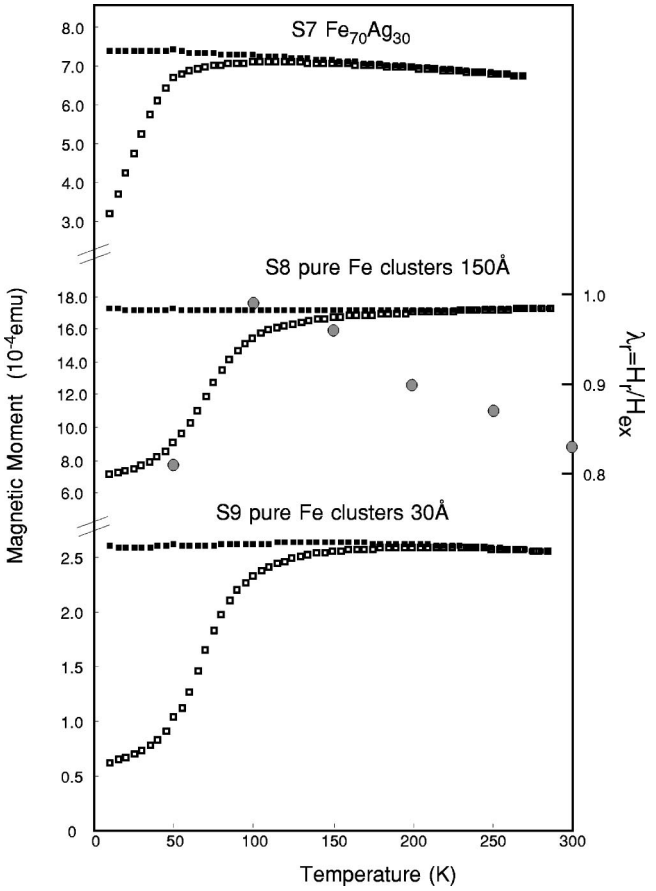

FIG. 11. FC/ZFC data taken at 500 G for samples S7–S9 in which there is strong interaction between the clusters. The ZFC curves are all characteristic of the formation of correlated spin glasses above ~50 K. The gray circles plotted on the data for S8 show the value of λ_r, obtained from the optimized fits to the approach to saturation using Eq. (9), at each temperature. The transition to the spin glass occurs at a critical value of $\lambda_r = 1$. The point at 50 K is the result of a poor fit due to the fact that the sample is no longer in the CSSG state.

using Eq. (9) start to fail (i.e., produce poor agreement). As shown in Fig. 9, an excellent fit is obtained at 2 K using Eq. (2) that assumes a random alignment of moments. It is concluded that decreasing the temperature from 300 to 2 K increases the particle anisotropy or decreases the exchange interaction so that λ_r increases through the critical value producing a transition from the CSSG state to a random alignment of supermoments as predicted by Chudnovsky *et al.*[49,51]

The changeover from the soft CSSG state to the random moment configuration is illustrated in the FC/ZFC curves of samples S7, S8, and S9 shown in Fig. 11. These all show a hardening in the ZFC data at low temperatures (~50 K). One can determine the variation of λ_r by fitting Eq. (9) to the measured approach to saturation at different temperatures. The result of this procedure for sample S8 is superimposed on FC/ZFC data for S8 in Fig. 11. It is evident that the formation of the CSSG, as shown by the magnetic softening in the ZFC data, occurs at the temperature at which λ_r crosses unity, as predicted by the RA model.

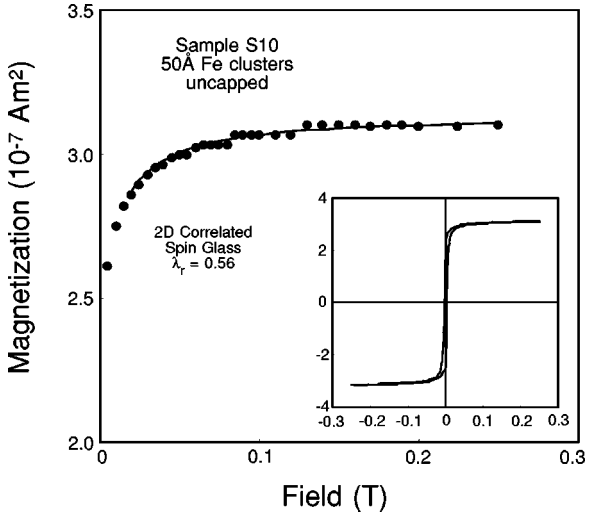

FIG. 12. Approach to saturation of S10 (uncapped 50-Å cluster film) at 2 K.

Both the anisotropy constant K_r and the exchange constant A vary with temperature through $M_s(T)$. Since A scales with M_s^2 and K_r with M_s^3 then λ_r is proportional to M_s and is thus expected to increase with decreasing temperature. The observed change is, however, much faster than M_s and another mechanism is required to explain the changeover from the CSSG to the random moment configuration. A similar transition has been observed in nanocrystaline films of pure Fe with a grain size ~12 nm produced by ball milling.[32] It was proposed that at low temperatures the particles decouple because an amorphous interface region between the grains forms an atomic spin glass that does not transmit exchange between the grains. In such a case there is a low-temperature disordered regime in which a collective freezing of the crystallite magnetic moments occurs. Despite the much smaller grain size in our samples and thus a severe restriction on the thickness of amorphous grain boundary this mechanism could also explain the apparent low-temperature decoupling since a much greater proportion of atoms are in the boundary phase. The CSSG fit parameters at high temperatures, however, indicate that it is mainly the anisotropy that is changing and not the exchange field as the temperature is reduced. An alternative mechanism could be a rapid increase in anisotropy due to the presence of the Ag buffer and capping layers. Since the samples are deposited with the substrates at room temperature the stress on the films will increase as the temperature deviates from 300 K.

This proposal is supported by the observation that, as shown in Fig. 12, good fits to the approach to saturation using the CSSG model [Eq. (8)] are obtained for the uncapped pure cluster sample (S10) all the way down to 2 K, i.e., it does not appear to show the low-temperature decoupling of the clusters. Note the change of the field scale in Fig. 12 and the very low coercivity of this sample relative to the Ag-capped ones. The λ_r value has only increased slightly relative to the room-temperature value as would be expected if there was no extra anisotropy-inducing mechanism. There are no FC/ZFC data available for this sample since it could not be transferred into the SQUID magnetometer without

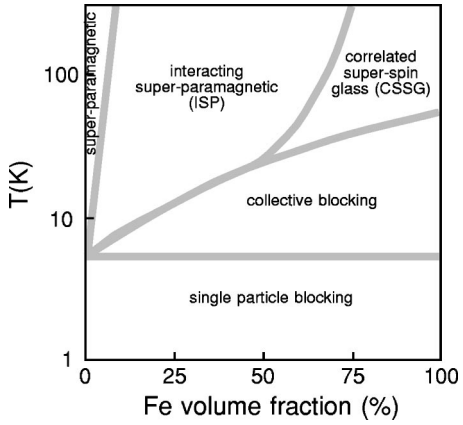

FIG. 13. Magnetic phase diagram of Ag-capped Fe nanoclusters (3 nm diameter) assembled in Ag matrices.

breaking vacuum so this finding cannot be independently verified, but it is additional evidence for the magnetoelastic mechanism producing the random supermoment to CSSG transition in the Ag-capped films.

V. SUMMARY AND CONCLUSIONS

Our results from the Ag-capped films can be summarized by the magnetic phase diagram shown in Fig. 13. We have investigated the magnetic behavior of nanostructured films produced by depositing, in UHV conditions, preformed Fe nanoclusters with a median diameter of 3 nm from a gas aggregation source in conjunction with atomic Ag vapor. In such films clusters can come into direct contact and interact via exchange. At very low volume fractions ($\sim 1\%$) and well above the cluster blocking temperature (~ 5 K) the films fulfill all the conditions for ideal superparamagnetism including an H/T scaling of the magnetization curves and a temperature-independent size distibution obtained by fitting Langevin functions to the data. The size distribution obtained in this way matches closely the one observed in STM images of the exposed clusters. At 2 K, the films demonstrate single-particle blocking and a remanence close to 50% indicating that the particles have a uniaxial anisotropy with a random directional distribution of axes. The anisotropy constant is 2.4×10^5 J m^{-3}.

At volume fractions up to 20%, i.e., below the percolation threshold, the high-temperature behavior can be described by a Curie-Weiss extension to the Langevin function described by Allia *et al.*[29] The magnetization data can be explained by assuming the sample consists of aggregates of clusters with their moments aligned by exchange and a dipolar interaction between the aggregates. At low temperature below a collective freezing of the moments the aggregates each have a uniaxial anisotropy axis in a random direction. The variation of the magnetic behavior as a function of volume fraction in the interacting films is well described by a MC simulation that includes dipolar and exchange interactions.

At high volume fractions ($>50\%$), above about 50 K the magnetic configuration is a correlated superspin glass. The Ag-capped films show a decoupling of the clusters at low temperatures so that the magnetization in each points along the local anisotropy axis. A similar phenomenon has been observed in nanostructured pure Fe films produced by ball milling[32] in which the decoupling was attributed to a loss of exchange coupling due to an amorphous boundary between the grains. Here we propose the effect is due to a large increase in the intracluster anisotropy arising from magnetoelastic stress induced by the Ag overlayer. This is supported by the observation that uncapped films measured in UHV do not show a similar decoupling and remain in the CSSG state at 2 K.

ACKNOWLEDGMENTS

We gratefully acknowledge support from the UK EPSRC (GR/L90026) and the EC (AMMARE Contract No. G5RD-CT-2001-0047P) for this work.

[1] E.C. Stoner and E.P. Wohlfarth, Philos. Trans. R. Soc. London, Ser. A **240**, 599 (1948).
[2] L. Néel, Ann. Geophys. (C.N.R.S.) **5**, 99 (1949).
[3] E.M. Chudnovsky and J.R. Friedman, Phys. Rev. Lett. **85**, 5206 (2000).
[4] B. Barbara, I. Chiorescu, R. Giraud, A.G.M. Jansen, and A. Caneschi, J. Phys. Soc. Jpn. **69**, 383 (2000).
[5] B. Barbara, L. Thomas, F. Lionti, I. Chiorescu, and A. Sulpice, J. Magn. Magn. Mater. **200**, 167 (1999).
[6] I.M.L. Billas, J.A. Becker, A. Châtelain, and W.A. de Heer, Phys. Rev. Lett. **71**, 4067 (1993).
[7] D.C. Douglass, A.J. Cox, J.P. Bucher, and L.A. Bloomfield, Phys. Rev. B **47**, 12 874 (1993).
[8] K.W. Edmonds, C. Binns, S.H. Baker, S.C. Thornton, C. Norris, J.B. Goedkoop, M. Finazzi, and N.B. Brookes, Phys. Rev. B **60**, 472 (1999).
[9] K.W. Edmonds, C. Binns, S.H. Baker, M.J. Maher, S.C. Thornton, O. Tjernberg, and N.B. Brookes, J. Magn. Magn. Mater. **231**, 113 (2001).
[10] K.W. Edmonds, C. Binns, S.H. Baker, M.J. Maher, S.C. Thornton, O. Tjernberg, and N.B. Brookes, J. Magn. Magn. Mater. **220**, 25 (2000).
[11] H.A. Dürr, S.S. Dhesi, E. Dudzik, D. Knabben, G. van der Laan, J.B. Goedkoop, and F.U. Hillebrecht, Phys. Rev. B **59**, 701 (1999).
[12] C. Binns, Surf. Sci. Rep. **44**, 1 (2001).
[13] C. Binns, S. Louch, S.H. Baker, K.W. Edmonds, M.J. Maher, and S.C. Thornton, IEEE Trans. Magn. **38**, 141 (2002).
[14] S. Tumanski, *Thin Film Magnetoresistive Sensors* (IOP Publishing, Bristol, 2001).
[15] J.I. Gittelman, B. Abelas, and S. Bozowski, Phys. Rev. B **9**, 3891 (1974).
[16] D. Fiorani, J.L. Tholence, and J.L. Dormann, Physica B **107**, 643 (1981).

[17] J.L. Dormann, L. Bessais, and D. Fiorani, J. Phys. C **21**, 2015 (1988).
[18] W. Luo, S.R. Nagel, T.F. Rosenbaum, and R.E. Rosensweig, Phys. Rev. Lett. **67**, 2721 (1991).
[19] R.W. Chantrell, M. El-Hilo, and K. O'Grady, IEEE Trans. Magn. **27**, 3507 (1991).
[20] M. El-Hilo, K. O'Grady, and R.W. Chantrell, J. Magn. Magn. Mater. **114**, 295 (1992).
[21] S. Gangopadhyay, G.C. Hadjipanayis, C.M. Sorensen, and K.J. Klabunde, IEEE Trans. Magn. **29**, 2619 (1993).
[22] K. O'Grady, M. El-Hilo, and R.W. Chantrell, IEEE Trans. Magn. **29**, 2608 (1993).
[23] S. Mørup and E. Tronc, Phys. Rev. Lett. **72**, 3278 (1994).
[24] S. Mørup, F. Bodker, P.V. Hendriksen, and S. Linderoth, Phys. Rev. B **52**, 287 (1995).
[25] C. Djurberg, P. Svedlindh, P. Nordblad, M.F. Hansen, F. Bødker, and S. Mørup, Phys. Rev. Lett. **79**, 5154 (1997).
[26] T. Jonsson, P. Svedlindh, and M.F. Hansen, Phys. Rev. Lett. **81**, 3976 (1998).
[27] J.L. Dormann, D. Fiorani, R. Cherkaoui, E. Tronc, F. Lucari, F. D'Orazio, L. Spinu, M. Nogues, H. Kachkachi, and J.P. Jolivet, J. Magn. Magn. Mater. **203**, 23 (1999).
[28] W. Kleemann, O. Petracic, Ch. Binek, G.N. Kakazei, Yu.G. Pogorelov, J.B. Sousa, S. Cardoso, and P.P. Freitas, Phys. Rev. B **63**, 134423 (2001).
[29] P. Allia, M. Coisson, P. Tiberto, F. Vinai, M. Knobel, M.A. Novak, and W.C. Nunes, Phys. Rev. B **64**, 144420 (2001).
[30] D.H. Ucko, Q.A. Pankhurst, and L. Fernandez Barquin, Phys. Rev. B **64**, 104433 (2001).
[31] D. Kechrakos and K.N. Trohidou, Phys. Rev. B **58**, 12 169 (1998).
[32] E. Bonetti, L. Del Bianco, D. Fiorani, D. Rinaldi, R. Caciuffo, and A. Hernando, Phys. Rev. Lett. **83**, 2829 (1999).
[33] L. Thomas, J. Tuaillon, J.P. Perez, V. Dupuis, A. Perez, and B. Barbara, J. Magn. Magn. Mater. **140**, 437 (1995).
[34] J.P. Perez, V. Dupuis, J. Tuaillon, A. Perez, V. Paillard, P. Melinon, M. Treilleux, L. Thomas, B. Barbara, and B. Bouchet-Fabre, J. Magn. Magn. Mater. **145**, 74 (1995).
[35] J.F. Löffler, H-B. Braun, and W. Wagner, Phys. Rev. Lett. **85**, 1990 (2000).
[36] J.M. Meldrim, Y. Qiang, Y. Liu, H. Haberland, and D.J. Sellmyer, J. Appl. Phys. **87**, 7013 (2000).
[37] D.A. Eastham, Y. Qiang, T.H. Maddock, J. Kraft, J.P. Schille, G.S. Thompson, and H. Haberland, J. Phys.: Condens. Matter **9**, L497 (1997).
[38] D.A. Eastham, P.M. Denby, A. Harrison, I.W. Kirkman, and A.G. Whittaker, J. Phys.: Condens. Matter **14**, 605 (2002).
[39] S.H. Baker, S.C. Thornton, K.W. Edmonds, M.J. Maher, C. Norris, and C. Binns, Rev. Sci. Instrum. **71**, 3178 (2000).
[40] M.D. Upward, B.N. Cotier, P. Moriarty, P.H. Beton, S.H. Baker, C. Binns, and K.W. Edmonds, J. Vac. Sci. Technol. B **18**, 2646 (2000).
[41] H. Haberland, Z. Insepov, and M. Moseler, Phys. Rev. B **51**, 11 061 (1995).
[42] C. Binns and M.J. Maher, New J. Phys. (to be published).
[43] M. Negrier, J. Tuaillon-Combes, V. Dupuis, P. Melinon, A. Perez, and A. Traverse, Philos. Mag. A **81**, 2855 (2001).
[44] D.A. Dimitrov and G.M. Wysin, Phys. Rev. B **54**, 9237 (1996).
[45] T.J. Jackson, C. Binns, E.M. Forgan, E. Morenzoni, Ch. Niedermayer, H. Glckler, A. Hofer, H. Luetkens, T. Prokscha, T.M. Riseman, A. Schatz, M. Birke, J. Litterst, G. Schatz, and H.P. Weber, J. Phys.: Condens. Matter **12**, 1399 (2000).
[46] D. Kechrakos and K.N. Trohidou, Phys. Rev. B **62**, 3941 (2000).
[47] J.L. Dormann, D. Fiorani, and M. El Yamani, Phys. Lett. A **120**, 95 (1987).
[48] E.M. Chudnovsky, J. Magn. Magn. Mater. **40**, 21 (1983).
[49] E.M. Chudnovsky, W.M. Saslow, and R.A. Serota, Phys. Rev. B **33**, 251 (1986).
[50] W.M. Saslow, Phys. Rev. B **35**, 3454 (1987).
[51] E.M. Chudnovsky, J. Appl. Phys. **64**, 5770 (1988).
[52] E.M. Chudnovsky, in *The Magnetism of Amorphous Metals and Alloys*, edited by J. A. Fernandez-Baca and Wai-Yim Ching (World Scientific, Singapore, 1995), Chap. 3.
[53] J. Tejada, B. Martinez, A. Labarta, and E.M. Chudnovsky, Phys. Rev. B **44**, 7698 (1991).
[54] J.F. Löffler, J.P. Meier, B. Doudin, J.-P. Ansermet, and W. Wagner, Phys. Rev. B **57**, 2915 (1998).